AIP | The Journal of Chemical Physics

A comparative study of the Au + H2, Au+ + H2, and Au− + H2 systems: Potential energy surfaces and dynamics of reactive collisions

Anaís Dorta-Urra, Alexandre Zanchet, Octavio Roncero, and Alfredo Aguado

Citation: The Journal of Chemical Physics **142**, 154301 (2015); doi: 10.1063/1.4916615
View online: http://dx.doi.org/10.1063/1.4916615
View Table of Contents: http://scitation.aip.org/content/aip/journal/jcp/142/15?ver=pdfcov
Published by the AIP Publishing

A comparative study of the Au + H_2, Au^+ + H_2, and Au^- + H_2 systems: Potential energy surfaces and dynamics of reactive collisions

Anaís Dorta-Urra,[1] Alexandre Zanchet,[2] Octavio Roncero,[2] and Alfredo Aguado[3]
[1]*Facultad de Ciencias Básicas y Aplicadas, Departamento de Física, Universidad Militar Nueva Granada, Bogotá DC, Colombia*
[2]*Instituto de Física Fundamental, CSIC Serrano 123, 28006 Madrid, Spain*
[3]*Facultad de Ciencias, Departamento de Química-Física Aplicada, Unidad Asociada CSIC-UAM, Universidad Autónoma de Madrid, 28049 Madrid, Spain*

(Received 12 November 2014; accepted 20 March 2015; published online 16 April 2015)

In order to study the Au^- + H_2 collision, a new global potential energy surface (PES) describing the ground electronic state of AuH_2^- system is developed and compared with the PESs of the neutral [Zanchet *et al.*, J. Chem. Phys. **132**, 034301 (2010)] and cationic systems [Anaís *et al.*, J. Chem. Phys. **135**, 091102 (2011)]. We found that Au^- − H_2 presents a H-Au-H insertion minimum attributed to the stabilization of the LUMO $3b_2$ orbital, which can be considered as the preamble of the chemisorption well appearing in larger gold clusters. While the LUMO orbital is stabilized, the HOMO $6a_1$ is destabilized, creating a barrier at the geometry where the energy orbitals' curves are crossing. In the anion, this HOMO is doubly occupied, while in the neutral system is half-filled and completely empty in the cation, explaining the gradual disappearance of the well and the barrier as the number of electrons decreases. The cation presents a well in the entrance channel partially explained by electrostatic interactions. The three systems' reactions are highly endothermic, by 1.66, 2.79, and 3.23 eV for AuH, AuH^+, and AuH^- products, respectively. The reaction dynamics is studied using quasi-classical trajectory method for the three systems. The one corresponding to the anionic system is new in this work. Collision energies between 1.00 and 8.00 eV, measured for the cation, are in good agreement with the simulated cross section for the AuH^+. It was also found that the total fragmentation, in three atoms, competes becoming dominant at sufficiently high energy. Here, we study the competition between the two different reaction pathways for the anionic, cationic, and neutral species, explaining the differences using a simple model based on the topology of the potential energy surfaces. © *2015 AIP Publishing LLC.* [http://dx.doi.org/10.1063/1.4916615]

I. INTRODUCTION

Gold is known to be a noble metal when associated in bulk phase[1] but can be reactive when encountered as nanoparticles,[2] which depending of the size and charge, can present catalytic activity.[3] The peculiar reactivity of gold is attributed to important relativistic effects, which makes the 6*s* and 5*d* orbitals become closer in energy than in other coinage atoms allowing efficient *sd* hybridization.[4] Recently, the effect of the size, geometry, and charge of small planar gold clusters on the dissociation barrier of H_2 has been studied.[5] It was found that H_2 is preferentially attached to sites with positive charge densities. The presence of such potential wells was found to be a necessary requirement for reaction to occur. This factor favors the reactivity of cationic clusters. However, a second requirement involves curve crossings with excited electronic states, which determines the height of the H_2 dissociation barrier. This crossing allows those anionic species with positive charge density sites to present lower barriers than neutral or cationic species. The accurate determination of the global Potential Energy Surface (PES) of the ground and excited electronic states makes possible a detailed study of the charge and curve crossing effects in the case of one gold atom. In addition, it allows us to compare our calculations with detailed gas-phase experimental results.[6–8] In the case of Au + H_2, a previous study has shown that a single neutral gold atom in the ground electronic state ([Xe] $4f^{14}5d^{10}6s^1, {}^2S$) presents very high barriers to react with H_2.[9] The PES of the ground electronic state presents a deep potential well which is considered the precursor of the chemisorption energy well appearing in gold nanoparticles, which originates from several curve crossings. In a similar study on the Au^+ + H_2 reaction, for the ground electronic state of Au^+ ([Xe] $4f^{14}5d^{10}, {}^1S$), where theoretical and experimental results were found in very good agreement,[10] it has been shown that a stable AuH_2^+ complex could be formed and was accessible without any barriers for this reaction marking a striking difference with the neutral case. To complete these two studies, involving the reactions of cationic and neutral gold with H_2, it is interesting to study the behavior of the anionic gold atom in the ground electronic state ([Xe] $4f^{14}5d^{10}6s^2, {}^1S$), with H_2, and compare the results with the neutral and cationic cases. These reactions are analogous to the reactions of H^+,[11] H ($1s^1, {}^2S$),[12] and H^- ($1s^2, {}^1S$)[13] with H_2 ($X^1\Sigma_g^+$), but with the difference that gold presents relativistic effects. The study of the anionic counterpart will help to understand the fact that anionic clusters with positive charge sites present lower barriers than neutral or cationic species, as reported in Ref. 5.

Moreover, it will allow us to fill the existing gap between the properties of isolated atoms and charged clusters, which is of fundamental importance for the future customization of their physicochemical properties.

For this reason, in this work, we will present a detailed study of the anionic system and we will see how the characteristics of the potential affects the reaction in comparison with the cationic and neutral case. The paper is organized as follows. First, in Sec. II, we will present the electronic structure calculations on the anionic system AuH_2^- and the principal characteristics of the PES. A comparison of the stable minimum for the AuH_2^- system and metastable minimum for the AuH_2 system with previous work[14] is also done. In Sec. III, the dynamics of the reaction $Au^- + H_2$ will be described and compared to the cationic and neutral cases. Finally, Sec. IV is devoted to extract some conclusions.

II. *AB INITIO* CALCULATIONS AND FIT

In the present work, the potential energy surface has been obtained for the ground electronic state of the $Au^- - H_2$ system to study the reaction $Au^-(^1S) + H_2(X^1\Sigma_g^+) \rightarrow AuH^-(X^2\Sigma^+) + H(^2S)$. For this purpose, we have performed electronic structure calculations using MOLPRO suite of programs.[15] For hydrogen atom description, the correlation-consistent polarized valence triple zeta basis set of Dunning[16] augmented with diffuse functions (aug-cc-pVTZ) was used. For the gold atom, the one-electron Gaussian-type basis sets ECP60MDF of the Stuttgart pseudopotential group[17] were used. Being a heavy element, relativistic effects have to be taken into account for a correct description of this atom. The ECP60MDF basis describes the 60 core electrons of the Au with an small-core fully relativistic effective core potential (RECP) and the remaining 19 electrons, 8 semicore ($5s^25p^6$) and 11 valence ($5d^{10}6s^1$) electrons, with a (12s12p9d3f2g)/[6s6p4d3f2g] Gaussian basis set. An *spdf* space was used. Looking for consistency, this methodology is the same that was previously employed for the endoergic $Au(^2S) + H_2(X^1\Sigma_g^+) \rightarrow AuH(X^1\Sigma^+) + H(^2S)$ and $Au^+(^1S) + H_2(X^1\Sigma_g^+) \rightarrow AuH^+(X^2\Sigma^+) + H(^2S)$ reactions.

The energy calculations were made at multireference configuration interaction (MRCI) level. The reference configurations were previously obtained with a multiconfigurational method, in particular with a state-averaged complete active space (SA-CASSCF)[18,19] method. The active space was taken for the 21 electrons of the neutral system ($Au + H_2$). The molecular orbitals (MOs) correlating with $5d, 6s$, and $6p$ atomic orbitals of the Au anion were used to determine the valence space, because this allows to describe the ground electronic state ^2S and excited states ^2D and ^2P of the gold atom. It has been seen that they play a role in the formation of the complex. All calculations were performed in C_s symmetry, to avoid the use of different active spaces in the CASSCF. In the C_s symmetry group, this active space is reduced to 9 orbitals of the irreducible representation A' and 4 of the A'' one. Adding 2 *s* orbitals for each hydrogen atom, the final result is an active space consisting in $11a'$ and $4a''$ orbitals.

Using the CASSCF orbitals for the neutral AuH_2 system, the ground electronic state X^1A' of the anionic system has been calculated using internally contracted MRCI (icMRCI) method[20,21] including single and double excitations. The reference configurations were recalculated for their appropriate number of electrons and multiplicity of the anionic system $Au^- + H_2$. Furthermore, the active space in the MRCI was reduced to $(10a', 4a'')$, because we verify that the $11a'$ orbital, which is higher in energy than the others, remains unoccupied in all reference configurations. Finally, a multireference Davidson correction technique (icMRCI + Q[22]) was applied to the final energies in order to approximately account for unlinked cluster effects of higher excitations.

TABLE I. Comparison of the $AuH^-(X^2\Sigma^+)$ and $H_2(X^1\Sigma_g^+)$ spectroscopic constants.

Diatom	Property	Expt.	ic-MRCI(+Q)
AuH^-	r_e/Å	1.597(6)[a]	1.626
	ω_e/cm^{-1}	⋯	1694
	D_0/eV	1.127[a]	1.26
H_2	r_e/Å	0.7414[b]	0.7441
	ω_e/cm^{-1}	4401[b]	4410
	D_e/eV	4.74[b]	4.74

[a]Experimental results from Ref. 24.
[b]Experimental results from Ref. 23.

To verify the accuracy of the *ab initio* computations with the scalar relativistic pseudopotential at the dissociation asymptotes, we have compared the calculated spectroscopic data with the experimental values for the diatomic molecules AuH^- and H_2. Table I shows the icMRCI+Q and experimental spectroscopic constants for the ground electronic states of the AuH^- and H_2 diatomic molecules, calculated in the supermolecule approach with the other atom (H and Au, respectively) at a distance of 10 Å. As can be seen, our results are in reasonable agreement with the experimental values.[23,24]

A. Global potential energy surface

The geometry of the AuH_2^- system is described in reactants' Jacobi coordinates, defined by the vector **r** between the two hydrogen atoms, the vector **R** that points from the H_2 center of mass to the Au atom, and the angle between the two vectors, γ. About 8000 *ab initio* points have been calculated in the intervals $|\mathbf{r}| = r \in [0.4\text{–}5$ Å$]$, $|\mathbf{R}| = R \in [0\text{–}5$ Å$]$, and $\gamma \in [0°\text{–}90°]$. A fit to the 8000 *ab initio* icMRCI+Q energies for the ground $^1A'$ electronic state has been done using the GFIT3C procedure introduced in Refs. 12, 25, and 26. The global PES is represented by a many-body expansion

$$V_{ABC} = \sum_A V_A^{(1)} + \sum_{AB} V_{AB}^{(2)}(r_{AB}) + V_{ABC}^{(3)}(r_{AB}, r_{AC}, r_{BC}),$$

where $V_A^{(1)}$ represents the energy of the atoms ($A = Au^q, H, H$ with $q = 0, 1$ or -1) in the ground electronic state, $V_{AB}^{(2)}$ represents the diatomic terms ($AB = AuH^q, AuH^q, HH$), and $V_{ABC}^{(3)}$ represents the triatomic one ($ABC = AuHH^q$).

The diatomic terms are written as a sum of short- and long-range contributions. The short-range potential is defined as a shielded Coulomb potential, whereas the long-range term is a linear combination of modified Rydberg functions[27] defined

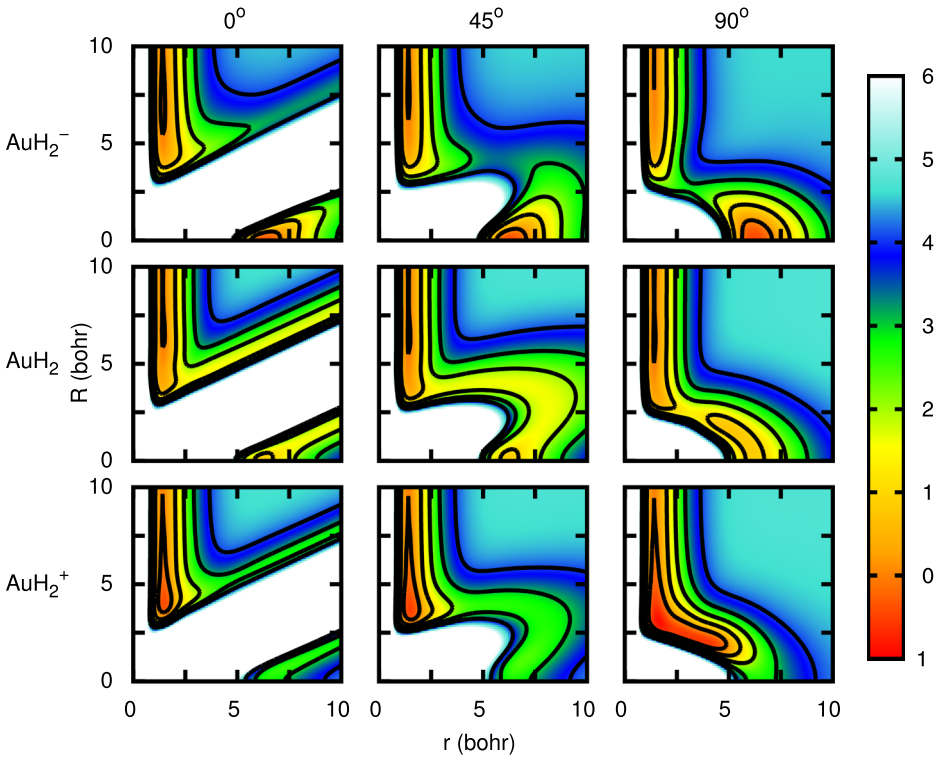

FIG. 1. Contour plots of the fitted $^1A'$ PES of AuH_2^-, AuH_2, and AuH_2^+ in Jacobi coordinates, for $\gamma = 0°$, 45°, and 90°, respectively. Energies are in eV.

as

$$\rho_{AB}(r_{AB}) = r_{AB}e^{-\beta_{AB}^{(2)}r_{AB}}, \qquad AB = \mathrm{AuH}^q, \mathrm{AuH}^q, \mathrm{HH},$$

with $\beta_{AB}^{(2)} > 0$.

The root-mean-square (rms) errors of the fitted diatomic potentials from *ab initio* values are 0.0039 eV and 0.018 eV for $AuH^-(X^2\Sigma^+)$ and $H_2(X^1\Sigma_g^+)$, respectively.

The three-body term is expressed as an expansion

$$V_{ABC}^{(3)}(r_{AB}, r_{AC}, r_{BC}) = \sum_{ijk}^{K} d_{ijk}\rho_{AB}^i\rho_{AC}^j\rho_{BC}^k$$

in the same type of modified Rydberg functions, but with exponents $\beta_{AB}^{(3)} > 0$. For ABB systems, like the AuH_2^q ones, there are only two non-linear parameters, $\beta_{AuH}^{(3)}$ and $\beta_{HH}^{(3)}$, and additional constraints[12,25,26] in the linear parameters, d_{ijk}. The linear parameters d_{ijk} $(i + j + k \le L)$ and the two non-linear parameters, $\beta_{AuH}^{(3)}$ and $\beta_{HH}^{(3)}$, are determined by fitting the calculated *ab initio* energies after subtraction of the one- and two-body contributions. The overall rms error of the fitted PES for the ground electronic state of AuH_2^- in the 8000 *ab initio* points is 0.052 eV. The PESs for the AuH_2 and AuH_2^+ ground electronic states have been previously developed (details can be found in Refs. 9 and 10, respectively).

B. Topological characteristics

To compare the PESs of these three systems, in Figure 1 are shown the contour plots of the PES obtained here for AuH_2^-, together with those corresponding to the neutral[9] and cationic[10] systems. In all the cases, the zero of energy corresponds to the asymptote in the entrance channel, i.e., to the gold atom far from H_2, and the hydrogen molecule at its equilibrium distance, r = 1.44 a.u. The anion presents an insertion well corresponding to a H-Au-H geometry, and $R = 0$ and $r \approx 6.00$ a.u. The calculated depth of this well, which corresponds to a stable species, is 0.49 eV. This result is in agreement with other theoretical previous,[14] calculating the difference between the bottom of the well and the reactants asymptote. The energy barrier height in the entrance channel of $Au^- + H_2$ is of 2.49 eV, as shown in Figure 2, and corresponds to an angle of 90° in the right top panel of Figure 1. A similar situation occurs for $Au + H_2$ system, but the barrier is lower and the well is shallower with a minimum above the $Au + H_2$ entrance channel, i.e., it is a metastable complex. On the contrary, the Au^+-H_2 cation does neither present the insertion well nor the barrier, but it presents a deeper

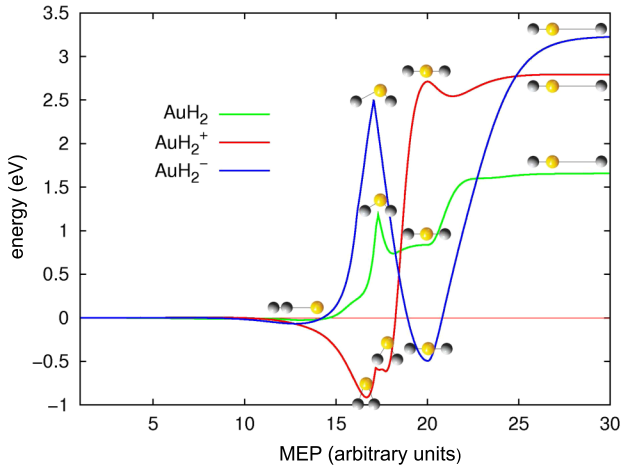

FIG. 2. MEPs for the $Au^q + H_2 \rightarrow AuH^q + H$ (q = 0, ±1) reactions. The zero of energy is in the reactants of each system. Note that the three reactions are endoergic by 1.66, 2.79, and 3.23 eV for the neutral, cationic, and anionic systems, respectively.

TABLE II. Stationary points of the AuH_2^- fitted ground electronic state.

Stationary point	R_{HH}/Å	R_{Au-H_2}/Å	γ/deg	Energy/eV
Reactants: $Au^-(^2S)+H_2(X^1\Sigma_g^+)$	0.74	⋯	⋯	0.00
Products: $AuH^-(^1\Sigma^+)+H(^2S)$	⋯	1.63	⋯	3.23
Transition state	1.15	1.48	90	2.49
Global minimum	3.31	0	⋯	−0.49
Entrance minimum	0.75	3.62	0	−0.07

well in the entrance channel, of −0.91 eV,[10] shown in the MEP (Minimum Energy Path) of Figure 2 and in the bottom panel of Figure 1. In order to summarize these features, the minimum energy path (in arbitrary units) joining $Au^q + H_2$ and $AuH^q + H$ rearrangements channels, for each $q = -1, 0, +1$ independently, is shown in Figure 2, and the stationary points features are listed in Table II. The important stationary points in the three systems present a T-shape geometry corresponding to the Jacobi angle $\gamma = 90°$, and from now on, we shall consider this angle as representative for the main features of the PESs of the three systems.

The progressive disappearance of the H-Au-H insertion well and the barrier when gradually varying the charge q, from the anion ($q = -1$), the neutral ($q = 0$), and the cation ($q = +1$), can be explained by the molecular orbitals energy, which, at first approximation, can be taken as being nearly the same for the three systems. The energies of the frontier orbitals follow a very similar pattern in $Au^- + H_2$ and $Au + H_2$ and can be described jointly. At long $Au^- + H_2$ distances, the doubly occupied HOMO orbital is the $6a_1$ (in C_{2v} symmetry for $\gamma = 90°$) correlates to the $6s$ orbital of Au^-, as it was the case for the neutral system.[9] As the two reactants approach, the energy of this orbital increases and at a distance of $R \approx 1.51$ Å (see Figure 2 of Ref. 9), the orbital crosses with the $3b_2$ LUMO orbital of $Au^- + H_2$ which is stabilized. This crossing corresponds to the top of the barrier appearing for the ground state potential energy. This can be easily seen by looking at the main electronic configurations contributions listed in Table III: for long and short R, there is only one electronic configuration with coefficients larger than 0.25, while at the crossing, there are three main configurations corresponding to different occupation numbers of the $5a_1$, $6a_1$, and $3b_2$ orbitals. These orbitals correlate to the $5d_{z^2}$, $6s$, and $6p_y$ atomic orbitals of the gold atom (when yz plane is used as reference).

Liu *et al.*[14] attributed the AuH_2^- well to a chemical bond between Au and $H\cdots H^-$. In this work, we interpret it as a consequence of the crossing between the $6a_1$ and $3b_2$ orbitals, allowing the formation of a bond between Au^- and each H atom. The $3b_2$ orbital correlates with the $6p_y$ orbital of Au^- which presents a favorable interaction with the σ_u anti-bonding orbital of H_2, explaining the stabilization of the mono-electronic energy term when forming a H-Au^--H linear complex. The energy of the orbitals and their amplitude densities are shown in Figures 2 and 3 of Ref. 9. The Mulliken atomic charge of −1.04 for the gold at the minimum geometry seems to corroborates our interpretation.

For the anionic case, the stability of the molecule has essentially used sp hybridization on Au^- to form two covalent bonds with the hydrogen atoms by allowing the double occupation of the stabilized $3b_2$ orbital. For the neutral case, the binding is weaker because there are now only three electrons in two bonding orbitals. For the cation, with only two electrons in these orbitals, it is no longer possible to form two covalent bonds and so the insertion complex is no longer stable.

By looking at the MEPs, it appears that the AuH^q products present a relatively high energy, corresponding to endothermic reactions in all the cases, being $\Delta E = 1.66$, 2.71, and 3.23 eV for the neutral, cationic, and anionic systems, respectively. The endothermicity is related to the dissociation energies of the diatomics, D_e, which are 3.07, 1.92, and 1.36 eV, for AuH, AuH^+ and AuH^-, respectively. These values are in agreement with the experimental one: 3.36, 2.13, and 1.13 eV.[23,24,32] We must point out that the dissociation energy of H_2 is slightly different in the three systems, because the ic-MRCI + Q is not size consistent. This small difference will produce a small shift in the opening of the total dissociation $Au^q + H + H$ channel, of about 0.10 eV, but is not expected to affect significantly the dynamics. The neutral AuH is more stable by ≈2.00 eV simply because the neutral Au atom has an unpaired electron which forms a covalent bond with atomic hydrogen. Au^+ and Au^- present a filled frontier orbital, what makes more difficult the formation of a covalent bond. As Au^- has its $5d$ and $6s$ orbitals completely filled, the interaction with H is less favorable than in the case of the cation which has only its $5d$ orbitals filled, and as a consequence, AuH^+ is more stable than AuH^-.

In the case of AuH_2^-, it is interesting to notice that there are two products channels, $AuH^- + H$ and $AuH + H^-$, with very similar energies as shown in Figure 3. In this figure, the zero of

TABLE III. Electronic configurations and main wave function expansion coefficients for the ground electronic state of the AuH_2^- system, in the C_{2v} symmetry point group.

Configurations	X^1A_1
$R = 9.01$ Å	
$\cdots(5a_1)^2(6a_1)^2(2b_2)^2(3b_2)^0$	0.912
$R = 3.62$ Å	
$\cdots(5a_1)^2(6a_1)^2(2b_2)^2(3b_2)^0$	0.904
$R = 1.51$ Å	
$\cdots(5a_1)^2(6a_1)^2(2b_2)^2(3b_2)^0$	−0.327
$\cdots(5a_1)^2(6a_1)^0(2b_2)^2(3b_2)^2$	0.789
$\cdots(5a_1)^1(6a_1)^1(2b_2)^2(3b_2)^2$	−0.306
$R = 0.51$ Å	
$\cdots(5a_1)^2(6a_1)^0(2b_2)^2(3b_2)^2$	0.910
$R = 0.10$ Å	
$\cdots(5a_1)^2(6a_1)^0(2b_2)^2(3b_2)^2$	0.913

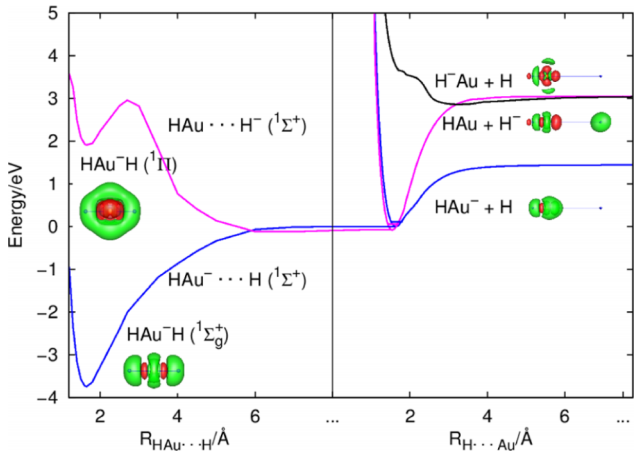

FIG. 3. Ground electronic state (in blue) and first excited state (in pink) in the $AuH^- + H$ and $AuH + H^-$ channels. In this figure, the zero of energy is in the $AuH^-(r_e) + H$ channel. Electronic density deformations for the anionic system are shown. This magnitude is obtained by subtracting the density associated to the isolated and neutral atoms from that of the AuH_2^- anion. Green/red colours are associated to positive/negative density difference.

energy is in the $AuH^-(r_e) + H$ minimum, which lies 3.23 eV higher than the $Au^- + H_2(r_e)$ energy used as zero in Figure 2. The experimental difference between the two channels can be obtained from the difference between the electron affinities (EAs), EA(AuH) = 0.758 eV[24] and EA(H) = 0.754 eV,[28] giving 0.004 eV, including the Zero Point Energy (ZPE). The difference between $AuH^-(r_e) + H$ and $AuH(r'_e) + H^-$ potential energies (with no ZPE) shown in Figure 3 is −0.08 eV (0.29 eV, if the Davidson correction is not considered). The ZPE of AuH and AuH^- is 0.138 and 0.108 eV, respectively. Thus, the theoretical energy difference between the two channels is −0.050 eV, when ZPE is included, larger than the experimental value of +0.004 eV. This small error arises from the electron affinity of AuH and H and are due to the incompleteness of the basis set. A complete description of these two channels would require furthermore a simultaneous treatment of both states including their mutual couplings. Such treatment, necessary to describe the charge transfer correctly, is not necessary in the scope of this work and would have been computationally prohibitive in order to construct the global PES of the system. It is however interesting to point out that a similar behaviour can be found in other triatomic systems, like the H_3^+ system, where the charge transfer occurs between $H_2 + H^+$ and $H_2^+ + H$ (see Figure 3 of Ref. 29).

The $AuH^-(X^2\Sigma^+) + H(^2S)$ asymptote corresponds to an interaction between two open-shell subsystems, giving an attractive potential. However, in the $AuH(^1\Sigma^+) + H^-(^1S)$ channel, the interaction between two closed-shell subsystems gives a repulsive potential, as shown in Figure 3. To analyze the charge distribution along these channels, we calculate the electronic density deformation with respect to the density of the isolated and neutral atoms, placed at the same positions.[5,30] This explains that in the H-Au⁻-H well, the negative charge is distributed in the three atoms. Moreover, the crossing takes place at relatively long distances at which we expect that the charge transfer becomes inefficient. By this reason, here, we shall neglect this charge transfer and only consider the $AuH^-(X^2\Sigma^+) + H(^2S)$ channel, which is the one with lower energy at short distances. Note that there is a conical intersection between the first and second excited states, which corresponds to a $^1\Sigma^+ - {}^1\Pi$ crossing.

III. THE QUASICLASSICAL TRAJECTORY METHOD

In this section, we present a systematic study on the $Au^- + H_2 \rightarrow AuH^- + H$ reactive collision in the ground electronic state and a comparison with the dynamics of the corresponding neutral and cationic systems, previously presented in Refs. 9 and 10. We will focus on a broad energy interval, including energies up to 12.0 eV. For this purpose, a standard quasiclassical trajectory method (QCT) is used.[31] The classical equations of motion were solved using the Hamiltonian associated to the two Jacobi vectors, **r** and **R**, expressed in cartesian coordinates as

$$H = \frac{1}{2m}\sum_{i=1}^{3} p_i^2 + \frac{1}{2\mu}\sum_{i=4}^{6} p_i^2 + V(q_1, q_2, \ldots, q_6), \qquad (1)$$

with $q = \{r_x, r_y, r_z, R_x, R_y, R_z\}$, and where $m = m_B m_C/(m_B + m_C)$ and $\mu = m_A(m_B + m_C)/(m_A + m_B + m_C)$ are the reduced masses associated to **r** and **R**, respectively. The corresponding Hamilton equations were derived in generalized coordinates as

$$\frac{dq_i}{dt} = \frac{\partial H}{\partial p_i}, \qquad \frac{dp_i}{dt} = -\frac{\partial H}{\partial q_i} = -\frac{\partial V}{\partial q_i}, \quad i = 1, \ldots, 6. \qquad (2)$$

Quantization in the initial BC diatomic fragments was done as follows. First, one of the radial classical turning points was chosen at the energy of the quantum vibrational state. The initial rotational angular momentum was set perpendicular to the axis of the BC molecule according to Ref. 31. The trajectories were started at an initial distance R_{ini}, adding an interval $\alpha T v$, where T is the vibrational period, v is the initial velocity between A and BC, and $\alpha \in [0, 1]$ is a random number.[31] The integration over the initial conditions was done using a Monte Carlo sampling, as introduced by Karplus *et al.*[31] to get the cross sections.

The final conditions were set as follows. First, the distances among all diatomic fragments were calculated. If the three distances were longer than the corresponding dissociation distance, R_{dis}, and the corresponding "diatomic" radial energies were above the dissociation energy, then the trajectory was assigned to the complete dissociation channel. If this conditions was not fulfilled, the quantum numbers for the diatomic fragment were determined in a two step procedure. First, the rotational quantum number was set by determining the classical angular momentum and discretizing it to the closest integer value, j. Second, the total internal diatomic energy, rotation, and vibration were compared to the quantum rovibrational eigenvalues associated to j. Dealing with very excited vibrational states, the standard rigid rotor or normal modes' approaches were not valid. For this reason, the quantum rovibrational states of all diatomic fragments were calculated numerically using a Numerov method on a radial grid of 5000 points. These calculations were implemented in the code miQCT3, already used to treat the cationic system.[10]

Calculations were performed for the ground rovibrational state of H_2 ($v = 0$, $j = 0$) and for collision energies sampled between 0.60 and 12.0 eV. The step adaptive Adams method (average step 0.05 fs) was used to integrate the set of Hamilton equations, and the conservation of both the total energy and angular momentum was carefully checked. At each step, relative precision of 10^{-12} for the distances and the momenta was required, yielding to a conservation of total energy and total angular momentum with average errors of 10^{-4} eV and $10^{-5}\hbar$, respectively. The high number of trajectories per batch, $N = 100\,000$, gives a maximal statistical Monte Carlo error on reaction probability lower than 1% in all the cases.

Once all trajectories are calculated, the reaction cross section for a given collision energy E_{col} and rovibrational initial state (v, j) can then be written as

$$\sigma_{vj} = \pi b_{max}^2 P_\lambda, \tag{3}$$

where b_{max} is the maximum value of the impact parameter leading to reaction, and P_λ is the reaction probability on a given channel λ is defined as

$$P_\lambda(E) = \frac{N_\lambda}{N_t}, \tag{4}$$

where N_t is the total number of trajectories calculated with initial impact parameter lower than b_{max}, and N_λ is the number of trajectories leading to reaction.

IV. COLLISIONAL RESULTS AND DISCUSSION

The three systems under study present a rather high endothermicity and require high collision energies to react to form hydride products,

$$Au^q + H_2 \rightarrow AuH^q + H. \tag{5}$$

This reaction was simulated for the neutral system[9] and the reaction cross section increases up to a collision energy of 3.00 eV, presenting a reaction threshold of ≈1.60 eV. The AuH products were essentially in its ground vibrational state, and a little of vibrational excitation of the products was obtained as total energy increases. On the contrary, the products were rotationally very excited, what was interpreted in term of the H + LL → HL + L character of the reaction (here, H and L stand for heavy and light, respectively). Later, Li *et al.*[32] measured the cross section of AuH^+ products in the $Au^+ + H_2$ reaction and deuterated analogues, up to very high collision energies, of 8.00 eV, well above the total fragmentation threshold, at ≈4.50 eV, leading to

$$Au^+ + H_2 \rightarrow Au^+ + H + H. \tag{6}$$

The experimental cross section to form AuH^+ products presents a peak about 4.60 eV, close to the total dissociation threshold and was very nicely reproduced by QCT simulations on a new three-dimensional PES.[10] In these simulations, it was found that after 4.50 eV, the total fragmentation channel cross section increases rapidly with increasing energy, becoming dominant after 5.10 eV, and of the same order.

In this work, we focus on the competition of the reaction channel, Eq. (5), and the total dissociation channel, Eq. (6). In Figure 4, we present the cross sections for these two channels

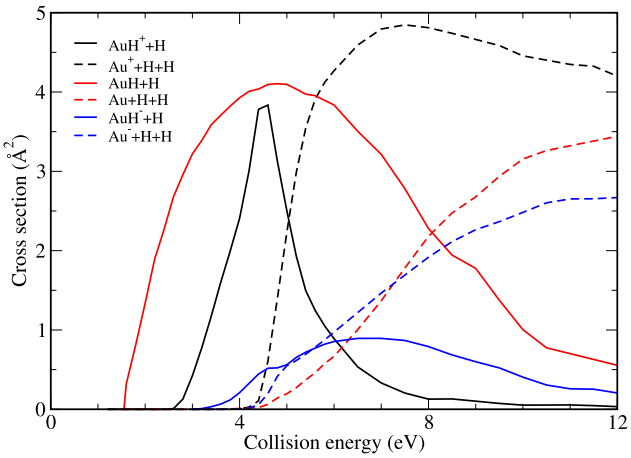

FIG. 4. Total cross sections of the hydride formation (solid) and total dissociation (dashed) for the $Au^q + H_2$ collision, with $q = -1$, 0 and +1.

for the $Au^q + H_2$ ($v = 0$, $j = 0$) collisions. The reaction cross section for the formation of the hydride presents a maximum for the three system, as previously reported for $Au^+ + H_2$.[10,32] The position, height, and width of the cross section strongly depends on the system, while the total dissociation channel opens at ≈4.50 eV in all cases, the dissociation energy of H_2.

In the case of $Au^+ + H_2$, the total dissociation mechanism is very efficient and its cross section rises very quickly with energy once the total dissociation channel opens (~4.50 eV), and it reaches a maximum of 4.85 Å around a collision energy of 7.50 eV before dropping very smoothly. As a result, the hydride formation cross section presents its maximum when the total dissociation channel opens and then drops very quickly giving a very sharp shape to the cross section curve, in quite good agreement with the measured cross section.[10,32]

The total dissociation cross section obtained in the neutral case, $Au + H_2$, increases more smoothly with collision energy, and at 12.0 eV, the cross section does not seem to have reached the maximum. As a consequence, the hydride formation cross section presents its maximum around 5.00 eV, with a much broader peak. This broader peak indicates that the two processes compete in a larger energy interval, either because the total fragmentation is less efficient or because the hydride formation is more efficient. It is interesting to point out here that the maximal cross section of the hydride formation in the cationic and neutral cases is very similar. However, in the energy range of 4.00–6.00 eV, the reaction probability in the neutral case (calculated in this work to be ≈70%) is considerably higher than in the cationic case (calculated in this work to be ≈50%). This difference in reaction probabilities is compensated by the maximal impact parameter which is higher in the cationic case (≈1.60 Å versus ≈1.30 Å) due to the presence of the relatively deep well in the entrance channel which allows longer range interactions.

In the anionic case, $Au^- + H_2$, the hydride formation cross section is considerably lower than the other two cases. The maximum of the cross section is ≈0.90 $Å^2$ compared to ≈4.00 $Å^2$ for the neutral and cationic systems. This low cross section is associated to a rather low reaction probability in the corresponding energy range (calculated in this work to be

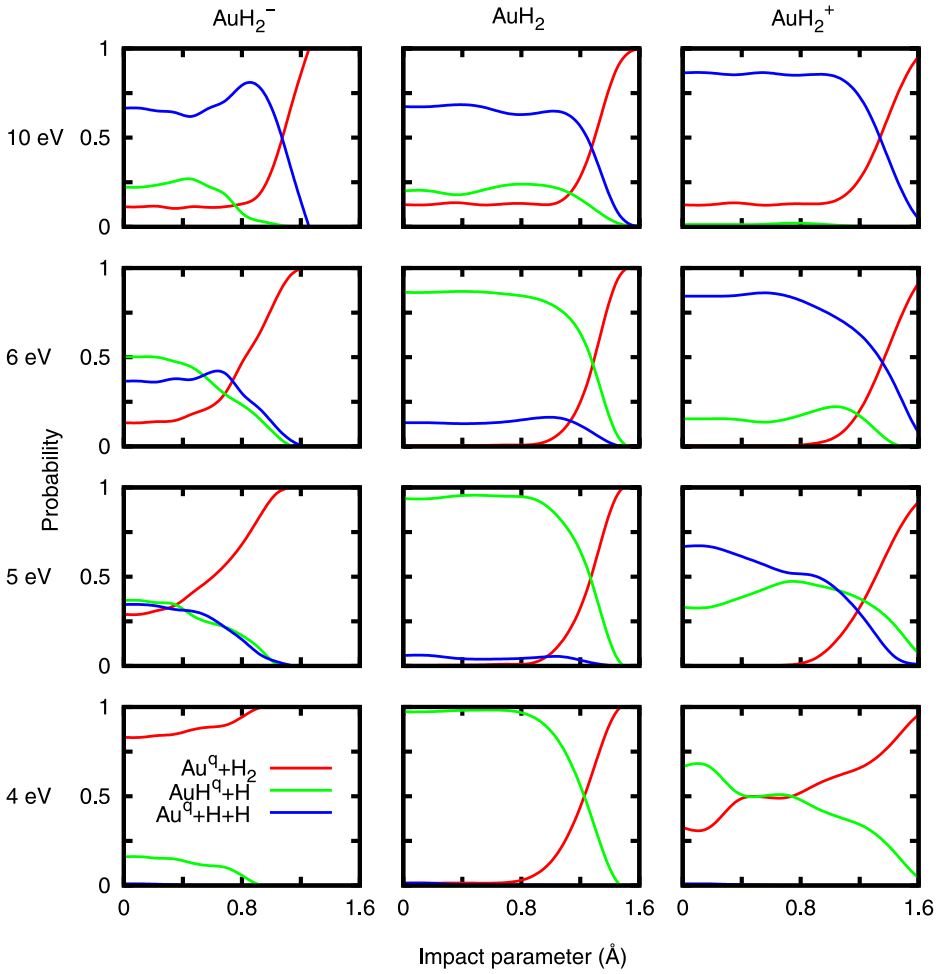

FIG. 5. Probabilities of forming the different products as a function of impact parameter for the $Au^- + H_2$ (left), $Au + H_2$ (center) and $Au^+ + H_2$ (right) reactions for collisions energies of 4.00, 5.00, 6.00 and 10.0 eV from bottom to top panels.

≈15%) and a smaller maximal impact parameter (≈1.00 Å). The total dissociation cross section however is comparable to that of the neutral system indicating that the efficiency of the process is similar in these two cases, but different from the cationic case. In the neutral and cationic systems, the reaction dynamics mechanism presents a competition between two processes, the hydride formation and total fragmentation, as can be seen in Figure 4. In the anionic one, this is not the case, because the hydride formation is four times lower, and the total dissociation mechanism seems to dominate in all the energy interval studied.

These results can be rationalized in terms of two different factors, the reaction probability, P_λ, and the maximum impact parameter, b_{max}, as illustrated in Eq. (3). The reaction probability may be related to the number of vibrational eigenstates of each of the products. AuH, AuH^+, and AuH^- have 20, 15, and 14 vibrational levels, respectively. This could explain why the probability for forming AuH is considerably larger (≈70%) than for AuH^+ (≈50%) and AuH^- (≈15%). However, as the difference between the cation and anion is too large to be attributed to this argument, we think that the repulsive long range potential in the anion case prevents Au^- to get close to H_2 leading to a drop in reaction probability.

The formation of hydrides can be better understood looking at Figure 5, which presents the probabilities to form the different products as a function of the impact parameter at different collision energies. It can be seen that for a collision energy of 4.00 eV, the three systems have a completely different behaviour when the total dissociation channel is still not open. The anionic system has a low reaction probability, even at low impact parameter. The neutral system has a very high reaction probability, nearly one at low impact parameters up to 0.80 Å, then it drops linearly down to 0 at ≈1.40 Å. The cationic system is an intermediate case, the reaction probability is around 70% at low impact parameters then drops progressively at 50% for b = 0.40 Å and remains constant up to b = 0.80 Å. For higher impact parameters, the probability drops then very slowly to 0 at b = 1.63 Å.

When the collision energy reaches 5.00 eV, the hydride probability in the neutral system remains identical and only a small portion leads to total dissociation when this channel opens. In the ionic systems, however, the changes are more important. In the anion, the inelastic probability (leading back to $Au^- + H_2$) falls considerably, while the probabilities of reactive collisions (hydride formation and total dissociation) rises considerably. As a result, at low impact parameters, up to $b \approx 0.40$ Å, the probabilities of the three products are similar. As the impact parameter increases, the probabilities of the hydride formation and total dissociation drop progressively to 0 at $b \approx 1.00$ Å, both in the same way. In the cationic system, the changes are also important. For impact parameters lower than 0.80 Å, the inelastic probability falls to nearly 0 and the probability to form the hydride drops significantly. This is due to a particularly efficient total dissociation mechanism

which becomes the dominant process up to $b = 1.00$ Å. For higher impact parameters, the total dissociation becomes less favorable and its probability start to drop faster than the hydride formation one.

When the collision increases to 6.00 eV, the evolution of the different probabilities follows the same trend as before. In the neutral system, the inelastic probability remains nearly unchanged while a greater portion of the reactive collisions leads to total dissociation. The hydride formation however still remains the dominant process as the progression of the effectivity of the total dissociation mechanism is quite slow as discussed earlier. In the anionic system, the two reactive processes become more efficient than for a collision energy of 5.00 eV. However, for greater energies, this two reactive processes are no longer equi-probable. In the cationic system, the inelastic probability remains very low, and the total dissociation becomes the most efficient mechanism.

For the higher collision energies, the three systems start to behave in a more similar way. This can be seen looking at the probabilities at 10.0 eV collision energy. In all the cases, the total dissociation mechanism becomes dominant nearly up to the respective maximal impact parameters. Also, the inelastic probability is nearly the same in the three cases, and of the order of 10%. At this energy range, the details of the PES become irrelevant, and when the two reactants collide, total dissociation nearly always occur, and only those cases in which Au^q miss the H_2 target produce some inelastic collisions.

As the masses and initial conditions are identical in the three systems, the differences are attributed to the topological properties of the different PESs. A first clue can be found by comparing the three potentials in entrance channels ($\mathbf{r}_{HH}$ in its equilibrium distance) in polar coordinates as shown in Figure 6. These plots describe the potential energy of gold atom while approaching H_2 and will thus have a direct influence on the maximum impact parameter at which reaction occurs. The cationic system presents a well in the entrance channel accessible without any barriers. The attractive long range interaction induced by the well in the case of the cation deviates the trajectories making the reagents collide, thus leading to larger maximal impact parameters. On the other hand, the repulsive potential acts over the neutral and anion gold while approaching to the H_2. The potential over the anion is more isotropic (it nearly "sees" the H_2 molecule as a sphere) and more repulsive than the neutral atom. As a result, the trajectories with higher impact parameters are deflected and the maximal impact parameter is smaller than in the neutral case.

The entrance channel will also have a direct influence on the geometry of the first impact. To check this effect, we represented in Figure 7 the reaction probabilities to reach a given channel as a function of the Jacobi angle at the moment of the impact, $P_\lambda(\gamma_i)$ (with $\lambda \equiv$ inelastic, hydride formation, and total dissociation). For this purpose, we consider that the impact occurs when the modulus of the **R** vector reaches its first minimum, and the angle of impact, γ_i, is then defined as the angle between $\mathbf{r}_{H_aH_b}$ and the vector **R**. Considering high collision energies, this definition is quite useful as it allows us to implicitly take into account the gold penetration in the potential of H_2. Intuitively, one could think that the probabilities will depend strongly on the interaction potential, showing important differences in the angle of impact between the cation and the other two systems. However, these probabilities show a quite similar behavior as a function of the angle of impact for the cationic and neutral systems: they show a high proportion of impacts around 90° for all the collision energies. This seems to indicate that the dominant mechanism to reorient the H_2 is not necessarily the well, but more likely the shape of the repulsive potential, what is reasonable because of the high energies considered. As can be seen in Figure 6, the repulsive part of the potential looks like a prolate ellipsoid in the cationic and neutral, while it is spherical in the anionic case. As a consequence, the trajectories with higher impact parameters will transmit a torque to H_2. While H_2 starts to rotate, the modulus of **R** continues to decrease and the Jacobi angle gets near to 90° at the moment we consider to be the impact. In the case of the anion, there is a less reorientation of the molecule. This is because the repulsive potential has a nearly spherical shape and the H_2 molecule reorients less. As a result, the angular distribution of the impacts is much less polarized in this system. At lower collision energies, it presents maxima near 0°and 180° which are in agreement with the distribution of impact parameter (proportional to b^2). At higher energies, the spherical shape of the repulsive potential is progressively disappearing to become ellipsoidal as the other cases, and as a consequence, impacts near to 90° become also dominant as can be seen looking at the angular distributions obtained for collision energy of 10.0 eV.

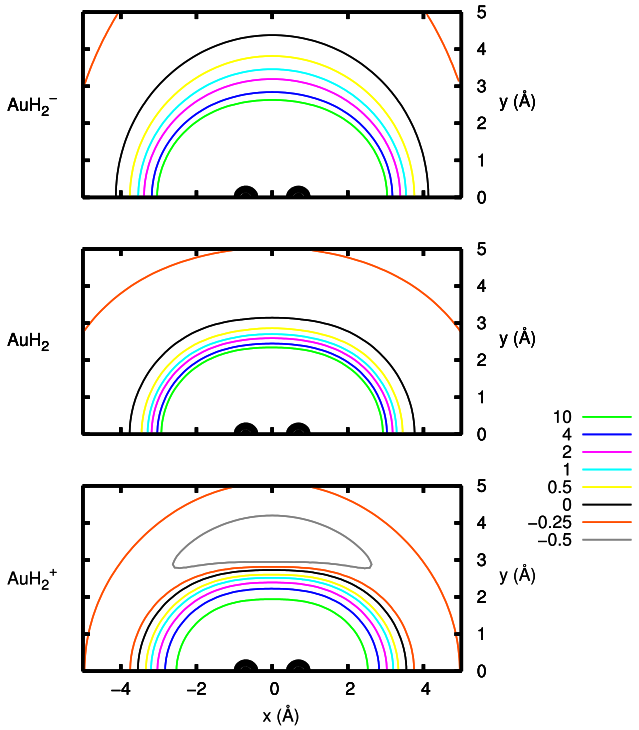

FIG. 6. Polar plots of the three systems showing the potential energy of gold atom near H_2 molecule in its equilibrium distance. Distances are represented in atomic units and isocontours in eV.

The reaction probability, $P_\lambda(\gamma_i)$, measures the probability of arriving to a particular γ_i at the moment of impact

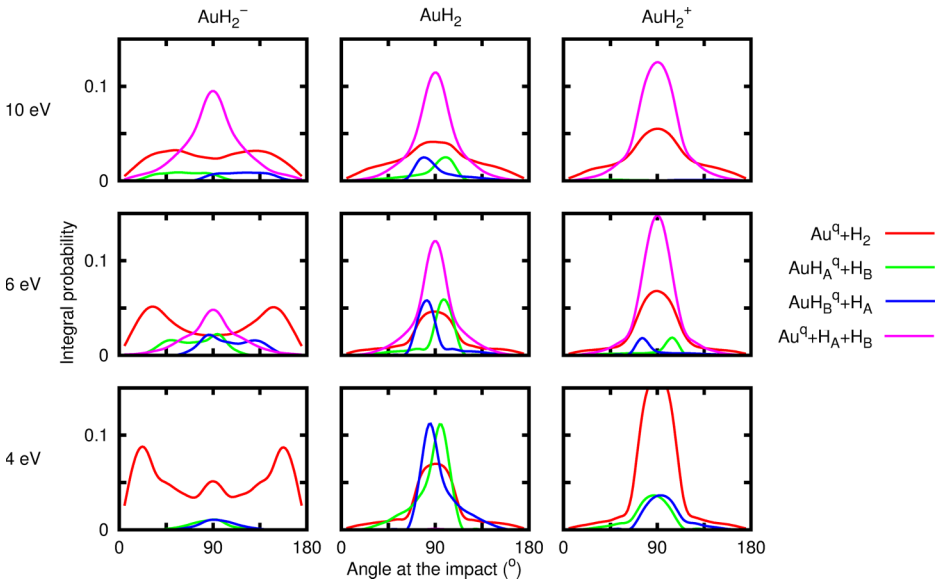

FIG. 7. Probability, $P_\lambda(\gamma_i)$, to reach an exit channel, λ, as a function of the Jacobi angle of the first impact, γ_i. Probabilities are shown for collision energies of 4.00 (bottom), 6.00 (center), and 10.00 eV (top) for the anionic, neutral, and cationic system (left to right panels, respectively).

multiplied by the probability of reaching each of the possible channels (inelastic, hydride formation, and total fragmentation) from this γ_i value. In order to get a direct information on how the reaction probability changes with the angle of impact, we define a new quantity $N_\lambda = P_\lambda/(P_i + P_h + P_d)$ (with $P_i, P_h, and P_d$ being the inelastic, hydride formation, and total dissociation probabilities, respectively). In Figure 8 are shown these new normalized probabilities, N_λ. In all the cases, the maximum probability of hydride formation and total dissociation is obtained when the first collision impact occurs at an angle of 90°. When the impact takes place near linearity ($\gamma = 0°$ or 180°), it is very unlikely to obtain a reactive collision. Another striking point is that there is a clear polarisation in the hydride formation probabilities. Green and blue curves show mirror symmetry with respect to 90°. This means that the hydride formation has a non-statistic behaviour, because if it was the case, both the $AuH_A + H_B$ and $AuH_B + H_A$ relative probabilities curves were equal.

This tells us that the process is essentially direct and that the first impact is governing the reaction. Furthermore, it appears that there are two different mechanisms. When the gold collides with one given H atom (approximately $\gamma < 70°$ or $> 110°$), if an hydride is formed, it is essentially with the other H atom, meaning that the principal mechanism in this case is a migration mechanism:[33,34] in the collision, a high torque is transferred to the H_2, making the first hydrogen to escape with high energy and angular momentum, leading the second hydrogen close to Au^q and without enough energy to dissociate, does forming AuH^q products.

When it collides between the two hydrogens (approximately $70° < \gamma < 110°$), the tendency is to form the hydride with the closest H atom at the moment of the impact, i.e., in this situation, the heavy Au^q drags the hydrogen atom it finds in its way, breaking the H_2 bond. In this situation, the energy is mainly transferred to the two hydrogen atoms, thus favoring the total dissociation channel. In the case of the cationic system, we can see in Figure 1 that at the Jacobi angle

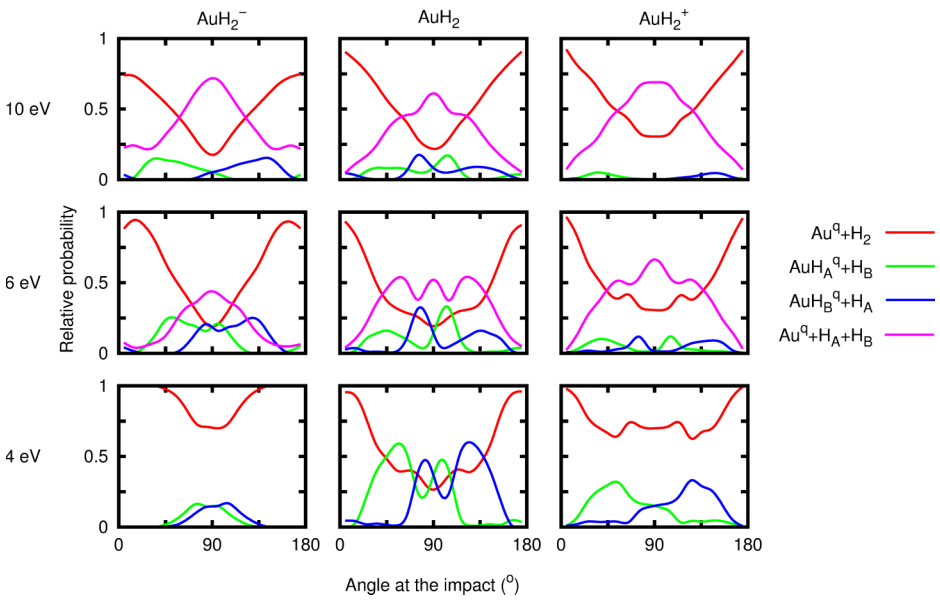

FIG. 8. Normalized probability, $N_\lambda(\gamma_i)$, to reach an exit channel, λ, as a function of the Jacobi angle of the first impact, γ_i. Probabilities are shown for collision energies of 4.00 (bottom), 6.00 (center), and 10.0 eV (top) for the anionic, neutral, and cationic system (left to right panels, respectively).

of 90°, the well in the entrance channel has an extension up to **r** values of 5 a.u., as a consequence, the energy is transferred to both H more efficiently than in the neutral system thus favoring the total dissociation. Moreover, in $Au^+ + H_2$ collisions at relatively low energies (4.00 eV), there is a marked effect of the well in the entrance channel, since it produces a very high probability of reaching angles close to 90°, as can be seen comparing the right-bottom panels of Figures 7 and 8.

V. CONCLUSIONS

In this work, we presented the PES for the ground electronic state of the AuH_2^- system. In order to obtain a global analytical hypersurface, we fitted around 8000 *ab initio* points calculated at MRCI-Q level. The reaction dynamics $Au^-(^1S) + H_2(X^1\Sigma_g^+) \rightarrow AuH^-(^2\Sigma^+) + H(^2S)$ and the results were compared with the corresponding ground state reaction of AuH_2 and AuH_2^+ systems.

We can conclude that the three reactions are endoergic by 1.66, 2.79, and 3.23 eV, respectively for the neutral, cationic, and anionic systems. In the entrance channel, the three systems present different topological characteristics. The cationic system exhibits a stable potential well of about −0.91 eV accessible without any barrier which is attributed to an electrostatic interaction. This interaction induces a partial transfer of electrons from H_2 to Au^+ atom, producing a considerably strong interaction. This behaviour is similar to what happens with planar gold clusters, where the H_2 can attach to the cluster when a gold atom presents a electrons deficit, as discussed in a previous work.[5] In the anionic and neutral systems, there is an energy barrier in this region of the MEP, and both systems present an insertion well due to the strong interaction of the *d* orbitals from gold with the antibonding orbital of H_2. As the gold cation does not have enough electrons to populate these orbitals, the antibonding orbital of H_2 cannot be stabilized, and no stable insertion complex can be formed. These mechanisms similar to what have been observed with planar gold clusters[5] can be studied more in details in a triatomic system, allowing a better understanding of the reactivity of H_2 and this kind of gold clusters.

The dynamical calculations, which take into account the vibrational energy of the diatomic molecules, show that the hydride channels, $AuH^q + H$, open at 1.53, 2.66, and 3.07 eV, respectively for the neutral, cationic, and anionic systems, and the total dissociation channel, $Au^q + H + H$, opens around 4.50 eV, in total agreement with the PES endothermicity. In the three systems, the total dissociation cross sections increase quickly with collision energy once the total dissociation channel is open, becoming the dominant mechanism at high collision energy. In the cationic system, it is even more favorable, and the cross section increases faster than the two other systems. The total dissociation mechanism is attributed to the prolate shape of the repulsive part of the PES. As a consequence, the cationic system, due to the well in the entrance channel, presents a more prolate shape of the repulsive potential and thus a more effective total dissociation mechanism. In the opposite way, the very spherical shape of the repulsive potential in the anionic system leads to a less effective total dissociation mechanism.

ACKNOWLEDGMENTS

This work has been supported by Comunidad Autónoma de Madrid (CAM) under Grant No. S2009/MAT/1467 and by Ministerio de Economía e Innovación under Project Nos. CSD2009-00038 and FIS2011-29596-C02. We also acknowledge the ICTS grants for computing time at CESGA supercomputer center. The authors want to thank the reviewers for their suggestions to improve the paper quality.

[1]B. Hammer and J. K. Norskov, Nature **376**, 238 (1995).
[2]M. Haruta, N. Yamada, T. Kobayashi, and S. Iijima, J. Catal. **115**, 301 (1989).
[3]R. Coquet, K. L. Howard, and D. J. Willock, Chem. Soc. Rev. **37**, 2046 (2008).
[4]H. Häkkinen, M. Moseler, and U. Landman, Phys. Rev. Lett. **89**, 033401 (2002).
[5]A. Zanchet, A. Dorta-Urra, A. Aguado, and O. Roncero, J. Phys. Chem. C **115**, 47 (2011).
[6]M. Ishida, R. Yamashiro, Y. Matsumoto, and K. Honma, J. Chem. Phys. **124**, 204316 (2006).
[7]J. J. Schroden, H. Floyd Davis, and C. A. Bayse, J. Phys. Chem. A **111**, 11421 (2007).
[8]P. B. Armentrout, Int. Rev. Phys. Chem. **90**, 115–148 (1990).
[9]A. Zanchet, O. Roncero, S. Omar, M. Paniagua, and A. Aguado, J. Chem. Phys. **132**, 034301 (2010).
[10]D.-U. Anaís, Z. Alexandre, R. Octavio, A. Alfredo, and P. B. Armentrout, J. Chem. Phys. **135**, 091102 (2011).
[11]A. Aguado, O. Roncero, C. Tablero, C. Sanz, and M. Paniagua, J. Chem. Phys. **112**, 1240 (2000).
[12]A. Aguado and M. Paniagua, J. Chem. Phys. **96**, 1265 (1992).
[13]A. K. Belyaev and A. S. Tiukanov, Chem. Phys. **220**, 43 (1997).
[14]H. T. Liu, Y. L. Wang, X. G. Wang, P. D. Dau, Z. A. Piazza, D. L. Huang, C. Q. Xu, J. Li, and L. S. Wang, Chem. Sci. **3**, 3286 (2012).
[15]H.-J. Werner, P. J. Knowles, G. Knizia, F. R. Manby, M. Schütz, P. Celani, T. Korona, R. Lindh, A. Mitrushenkov, G. Rauhut, K. R. Shamasundar, T. B. Adler, R. D. Amos, A. Bernhardsson, A. Berning, D. L. Cooper, M. J. O. Deegan, A. J. Dobbyn, F. Eckert, E. Goll, C. Hampel, A. Hesselmann, G. Hetzer, T. Hrenar, G. Jansen, C. Köppl, Y. Liu, A. W. Lloyd, R. A. Mata, A. J. May, S. J. McNicholas, W. Meyer, M. E. Mura, A. Nicklass, D. P. O'Neill, P. Palmieri, D. Peng, K. Pflüger, R. Pitzer, M. Reiher, T. Shiozaki, H. Stoll, A. J. Stone, R. Tarroni, T. Thorsteinsson, and M. Wang, MOLPRO, version 2012.1, a package of *ab initio* programs, 2012, see http://www.molpro.net.
[16]T. H. Dunning, Jr. J. Chem. Phys. **90**, 1007 (1988).
[17]D. Figgen, G. Rauhut, M. Dolg, and H. Stoll, Chem. Phys. **311**, 227–244 (2005).
[18]H.-J. Werner and P. J. Knowles, J. Chem. Phys. **82**, 5053 (1985).
[19]P. J. Knowles and H.-J. Werner, Chem. Phys. Lett. **115**, 259 (1985).
[20]H.-J. Werner and P. J. Knowles, J. Chem. Phys. **89**, 5803 (1988).
[21]P. J. Knowles and H.-J. Werner, Chem. Phys. Lett. **145**, 514 (1988).
[22]E. R. Davidson, J. Comput. Phys. **17**, 87 (1975).
[23]K. P. Huber and G. Herzberg, *Molecular Spectra and Molecular Structure*, Constants of Diatomic Molecules Vol. IV (Van Nostrand, Toronto, 1979).
[24]X. Wu, Z. Qin, H. Xie, R. Cong, A. Wu, Z. Tang, and H. Fan, J. Chem. Phys. **133**, 044303 (2010).
[25]A. Aguado, C. Suarez, and M. Paniagua, J. Chem. Phys. **98**, 308–315 (1993).
[26]A. Aguado, C. Tablero, and M. Paniagua, Comput. Phys. Commun. **108**, 259–266 (1998).
[27]R. Rydberg, Z. Phys. **73**, 376 (1931).
[28]K. R. Lykke, K. K. Murray, and W. C. Lineberger, Phys. Rev. A **43**, 6104 (1991).
[29]C. Sanz, O. Roncero, C. Tablero, A. Aguado, and M. Paniagua, J. Chem. Phys. **114**, 2182 (2001).
[30]L. González-Sánchez, S. Gómez-Carrasco, A. Aguado, M. Paniagua, M. L. Hernández, J. M. Alvariño, and O. Roncero, J. Chem. Phys. **121**, 9865 (2004).
[31]M. Karplus, R. N. Porter, and R. D. Sharma, J. Chem. Phys. **43**, 3259 (1965).
[32]F. Li, C. S. Hinton, M. Citir, F. Liu, and P. B. Armentrout, J. Chem. Phys. **134**, 024310 (2011).
[33]F. J. Aoiz, L. Bañares, V. J. Herrero, V. Sáez-Rábanos, K. Stark, and H.-J. Werner, J. Chem. Phys. **102**, 9248 (1995).
[34]F. J. Aoiz, L. Bañares, J. F. Castillo, M. Menéndez, D. Skouteris, and H.-J. Werner, J. Chem. Phys. **115**, 2074 (2001).